

## SOURCE 2.0 MODEL DEVELOPMENT: $\text{UO}_2$ THERMAL PROPERTIES

P.J. Reid

ALARA Research, Inc., 975 First Ave., Saint John NB

M.J. Richards

Hydro Québec, 1155 rue Metcalfe, Suite 880, Montreal QC

F.C. Iglesias, A.C. Brito

Ontario Hydro, 700 University Ave., Toronto ON

### Introduction

During analysis of CANDU postulated accidents, the reactor fuel is estimated to experience large temperature variations and to be exposed to a variety of environments from highly oxidized to mildly reducing (Reference [1]). The exposure of CANDU fuel to these environments and temperatures may affect fission product releases from the fuel and cause degradation of the fuel thermal properties. Thus, it is important to model  $\text{UO}_{2+x}$  thermal properties as a basis for predicting fuel behaviour during accidents.

New models for the thermal properties of  $\text{UO}_{2+x}$  (*i.e.*, heat capacity and thermal conductivity) have been jointly developed within the Canadian nuclear industry under the SOURCE 2.0 project (Reference [2]). SOURCE 2.0 is a safety analysis code which will model the necessary mechanisms required to calculate fission product release for a variety of accident scenarios, including large break loss of coolant accidents (LOCAs) with or without emergency core cooling. The goal of the model development is to generate models which are consistent with each other and phenomenologically based, insofar as that is possible given the state of theoretical understanding.

Urania heat capacity is modelled in three different temperature ( $T$ ) regimes:  $T < 2670 \text{ K}$ ,  $2670 \text{ K} < T < T_{\text{melt}}$  and  $T > T_{\text{melt}}$ . For temperatures less than 2670 K, the heat capacity is modelled as having components due to phonon excitation, lattice dilation, Schottky defects and electron-hole excitation. At 2670 K, the urania is assumed to undergo a Bredig transition, and above this temperature the urania behaves differently. A semi-empirical approach is taken to this high temperature solid urania regime: the small polaron component is still modelled explicitly (since it involves the U cations and the Bredig transition only affects the O sub-lattice) and the balance is empirically derived based on experimental enthalpy data. For liquid urania, a separate semi-empirical approach based on the experimental data is used. Urania thermal conductivity is modelled by assuming that three processes contribute to the thermal conductivity: phonon transport, electron-hole transport and thermal radiation. The models of phonon and electron-hole excitation in both the heat capacity and the thermal conductivity are fully consistent, with the electron-hole transport assumed to be governed by a small polaron transport model.

### Heat Capacity of $\text{UO}_{2+x}$

Heat capacity is defined as the amount of energy which is required to raise the temperature of a given mass of a material by a given temperature increment. The heat capacity which is determined by this model is  $C_p$ , the heat capacity at constant pressure, and is expressed in units of  $\text{J}/(\text{kg}\cdot\text{K})$ . Theoretical determinations of heat capacity generally are in terms of  $C_v$ , the heat capacity at constant volume, which is related to  $C_p$  through the following relation from Reference [3]:

$$C_p = C_v + \left[ \frac{\alpha^2 \cdot V}{\beta} \right] \cdot T$$

(1)

where:

$\alpha$  is the coefficient of volumetric thermal expansion [ $\text{K}^{-1}$ ]  
 $\beta$  is the coefficient of isothermal compressibility [ $\text{Pa}^{-1}$ ]

V is the inverse of the density [ $\text{m}^3/\text{kg}$ ]  
 T is the temperature [K]

Several different processes can come into play as a substance absorbs energy and its temperature increases. In the case of a crystalline solid, these are:

- 1) Increase in the number of charge carriers (*e.g.* conduction electrons and holes)
- 2) Vibrations of the molecules (*i.e.* acoustic mode lattice vibrations)
- 3) Internal vibrations of the atoms within each molecule (*i.e.* optical mode lattice vibrations)
- 4) Partial rotation of the molecules
- 5) Excitation of upper energy levels of the molecules
- 6) Miscellaneous effects (*i.e.* Frenkel and/or Schottky defects)

The acoustic modes of the lattice vibrations will be dominated by the vibration of the Uranium atoms, due to their high mass. The optical modes of the lattice vibrations will be dominated by the Oxygen atoms. Partial rotation of  $\text{UO}_2$  molecules does not occur due to the fact that the crystal structure of  $\text{UO}_2$  does not allow for molecular rotation on any significant scale. This assumption is justified on the basis that the heat capacity of urania can be fully described without any terms modelling molecular rotation. Excitation of upper energy levels does not occur until the fuel reaches very high temperatures, *i.e.*  $> 4500$  K (see Reference [4]).

#### $C_p$ due to Lattice Vibrations and Lattice Dilation in $\text{UO}_{2+x}$

Lattice vibrations are an important contributor to specific heat. Einstein's formalism, which is typically used in developing correlations for the heat capacity of  $\text{UO}_2$ , assumes that all of the oscillating particles have the same frequency of oscillation,  $\nu_E$ . If we define  $\Theta_E = h \cdot \nu_E / k_B$ , then the expression for  $C_v$  is:

$$C_v = 3 \cdot N \cdot k_B \cdot \left( \frac{\Theta_E}{T} \right)^2 \cdot \frac{e^{\Theta_E/T}}{(e^{\Theta_E/T} - 1)^2} \quad (2)$$

where:

$k_B$  is Boltzmann's constant [ $1.380662 \cdot 10^{-23}$  J/K]  
 N is the "atomic density", *i.e.* number of atoms per kg in the lattice [ $\text{kg}^{-1}$ ]

This model only applies to atomic vibrations in which the distribution of vibrational frequencies is such that the approximation of one average vibrational frequency is valid, such as is the case for optical phonon modes which have a very narrow band width. With the large mass difference between the Uranium and Oxygen atoms and with the strong bonding between these atoms,  $\text{UO}_2$  probably has such narrow band width optical modes. Optical modes are more important at high temperatures than they are at low temperatures.

As stated above, the Einstein formulation is usually used in developing heat capacity correlations for  $\text{UO}_2$ . Another model for heat capacity due to harmonic lattice vibrations is due to Debye. This model has a characteristic temperature, the Debye temperature,  $\Theta_D$ . This treatment gives an expression for  $C_v$  as follows:

$$C_v = 9 \cdot N \cdot k_B \cdot \left( \frac{T}{\Theta_D} \right)^3 \cdot \int_0^{\Theta_D/T} \frac{z^4 \cdot e^z}{(e^z - 1)^2} dz \quad (3)$$

where:

z is the expression,  $h \cdot \nu / (2 \cdot B \cdot k_B \cdot T)$   
 $\Theta_D$  is the Debye temperature [K]

Both the Debye and Einstein models of heat capacity are approximations. Based on measurements of atomic vibrations, Willis [5] has proposed a combination model in which the vibration of the U atoms is described using the

Debye formalism and the vibration of the O atoms using the Einstein formalism. This is based upon the observation that the characteristic temperatures of  $\text{UO}_2$  can be different, depending upon the type of excitation (*i.e.* optical or acoustic modes). This is the approach selected for use in the present model, as it does not require fitting to experimental data, but uses independently determined values of  $\Theta_E$  and  $\Theta_D$ , along with the assumption that the acoustic modes are due to vibration of U atoms and the optical modes are due to vibration of O atoms. The characteristic temperature for the optical modes,  $\Theta_E$ , has been determined to be 542 K in Reference [6] and the characteristic temperature for the acoustic modes,  $\Theta_D$ , has been determined to be 182 K in Reference [6]. Therefore:

$$C_v = 3 \cdot N(x) \cdot k_B \cdot \left[ \frac{1}{3+x} \cdot \left( \frac{3 \cdot T^3}{\Theta_D^3} \right) \cdot \int_0^{\Theta_D/T} \frac{z^4 \cdot e^z}{(e^z - 1)^2} dz + \frac{2+x}{3+x} \cdot \left( \frac{\Theta_E}{T} \right)^2 \cdot \frac{e^{\Theta_E/T}}{(e^{\Theta_E/T} - 1)^2} \right] \quad (4)$$

where:

- $x$  is the stoichiometric deviation [O/U-2]  
 $N(x)$  is the atomic density corresponding to this stoichiometric deviation [(atoms) per kg]

There are higher-order effects (anharmonic effects) which cause the lattice vibration component of  $C_v$  not to follow the form outlined above. In addition, this model is intended to calculate  $C_p$ , which is obtained from  $C_p = C_v + (\alpha^2 \cdot V / \beta) \cdot T$

Anharmonic vibrations add a term to the heat capacity which is approximately linear in temperature, and the constant of proportionality,  $C_{anh}$ , has been determined to be  $3.8144 \cdot 10^{-3} \text{ J/(kg} \cdot \text{K}^2)$  in Reference [7]. Reference [8] tabulates values of  $(\alpha^2 \cdot V / \beta) \cdot T$  for 100%TD  $\text{UO}_2$  over the temperature range 300-2500 K. These data can be fit to a quadratic equation which is constrained to pass through 0 J/(kg·K) at 0 K. These effects (anharmonicity and the relationship between  $C_v$  and  $C_p$ ) result in the following additional terms to the equation for the heat capacity:

$$C_p^{add} = C_{anh} \cdot T + \frac{C_{d1} \cdot T + C_{d2} \cdot T^2}{1 - P} \quad (5)$$

where:

- $C_p^{add}$  is the addition to the heat capacity due to anharmonic vibrations and lattice dilation [J/(kg·K)]  
 $C_{d1}$ - $C_{d2}$  are the coefficients describing the contribution due to lattice dilation ( $C_v/C_p$  relationship):  
 $[C_{d1} = (3.1721 \pm 0.1242) \cdot 10^{-3} \text{ J/(kg} \cdot \text{K}^2), C_{d2} = (1.4760 \pm 0.0063) \cdot 10^{-5} \text{ J/(kg} \cdot \text{K}^3)]$   
 $P$  is the fractional porosity of the  $\text{UO}_2$

Hence, the expression for  $C_p$  due to lattice vibrations and dilation in  $\text{UO}_{2\pm x}$  is:

$$C_p^{lat} = 3 \cdot N(x) \cdot k_B \cdot \left[ \frac{1}{3+x} \cdot \left( \frac{3 \cdot T^3}{\Theta_D^3} \right) \cdot \int_0^{\Theta_D/T} \frac{z^4 \cdot e^z}{(e^z - 1)^2} dz + \frac{2+x}{3+x} \cdot \left( \frac{\Theta_E}{T} \right)^2 \cdot \frac{e^{\Theta_E/T}}{(e^{\Theta_E/T} - 1)^2} \right] + C_{anh} \cdot T + \frac{C_{d1} \cdot T + C_{d2} \cdot T^2}{1 - P} \quad (6)$$

#### $C_p$ due to Electron Defects in $\text{UO}_{2\pm x}$

To a first approximation, Schottky defects are linear in temperature, and the constant of proportionality ( $C_{sch}$ ) has been determined in Reference [7] to be equal to  $1.081 \cdot 10^4 \text{ J/(kg} \cdot \text{K}^2)$ . Deviations from stoichiometry are assumed to have a negligible impact on this value, since it involves a correction to an effect which is itself only of second order in importance.

#### $C_p$ due to Small Polaron Excitation in $\text{UO}_{2\pm x}$

For  $\text{UO}_2$  temperatures  $> 2000 \text{ K}$ , the contributions to heat capacity described in the above sections do not completely account for the observed heat capacity of  $\text{UO}_2$ . The difference can be seen when experimental data for

UO<sub>2</sub> enthalpy is plotted along with the enthalpy which would be predicted based on the processes described above. Note that enthalpy is the integral over temperature of the heat capacity. Figure 2 shows this difference for the experimental data of Hein and Flagella (Reference [9]). This difference indicates that there is another process (or group of processes) which absorb energy as temperatures increase into this range.

One physical process which occurs in UO<sub>2+x</sub> in this temperature range is the thermally induced disproportionation of the cation (*i.e.* the U ion) sub-lattice, which is shown by the following equation



This process is referred to as small polaron excitation, because the extra electron and hole on the U<sup>3+</sup> and U<sup>5+</sup> ions, respectively, induce local polarisations of the lattice which act to screen the Coulomb interactions between the charges and the lattice. These screened charges, or small polarons, can hop from one cation site to another (Reference [10]). So this process is dependent on the presence of electron and/or hole charge carriers and upon the U cations being in their lattice positions. This process has been shown to be able to explain the electrical conductivity and Seebeck coefficient of UO<sub>2+x</sub> (Reference [11]). The magnitude of the effect on the heat capacity is shown in this section to be sufficient to explain the excess heat capacity for 2000 K < T < 2670 K. The heat capacity for temperatures above 2670 K must be dealt with differently than for temperatures below 2670 K. The assumption that this process is active is equivalent to assuming that UO<sub>2</sub> is a Mott insulator.

The electrons and holes which are generated by the disproportionation reaction add two energy bands to the electronic energy spectrum of UO<sub>2</sub>, at E<sub>u</sub> and E<sub>l</sub>. These two bands are separated by an energy gap ΔU [J]; ΔU = E<sub>3</sub> + E<sub>5</sub> - 2·E<sub>4</sub> = E<sub>u</sub> - E<sub>l</sub>. The numeric subscripts identify the U cations involved.

The molar concentrations of electrons and holes will obey the following equations (which are based on the law of conservation of charge and on the principles of thermodynamic equilibrium, respectively):

$$p = n + 2 \cdot x \quad (8)$$

$$\frac{n \cdot p}{(1 - n - p)^2} = \exp\left(\frac{-\Delta F}{k_B \cdot T}\right) \quad (9)$$

where:

- n is the molar concentration of electrons, *i.e.* of U<sup>3+</sup> ions [1/mol]
- p is the molar concentration of holes, *i.e.* of U<sup>5+</sup> ions [1/mol]
- ΔF is the change in (Helmholtz) free energy associated with the reaction in Equation (7);  
ΔF ≡ ΔU - T·ΔS [J](per ion)
- ΔS is the entropy difference associated with the reaction [J/K](per ion)

In order to determine the heat capacity from this process, use is made of the thermodynamic identity:

$$C_v^{sp} = -T \cdot \left( \frac{\partial^2 F^{sp}}{\partial T^2} \right)_v \quad (10)$$

where:

- F<sup>sp</sup> is the Helmholtz free energy per kg UO<sub>2</sub> in the system due to the reaction defined by Equation (7), [J/kg]; F<sup>sp</sup> = ΔF · {N<sub>U</sub> · (1 - n - p) / 2}
- C<sub>v</sub><sup>sp</sup> is the component of the heat capacity due to small polaron excitation [J/(kg·K)]
- N<sub>U</sub> is the number of U ions per kg UO<sub>2</sub> [atoms/kg]

Using Equation (9) to define ΔF and substituting into Equation (10), we obtain:

$$C_v^{sp} = -\frac{N_U}{2} \cdot k_B \cdot T \cdot \frac{d^2}{dT^2} \left\{ (1-n-p) \cdot T \cdot \ln \left[ \frac{(1-n-p)^2}{n \cdot p} \right] \right\} \quad (11)$$

Evaluation of the above derivative gives the following expression for  $C_v^{sp}$  (note that  $\frac{dp}{dT} = \frac{dn}{dT}$ ):

$$C_v^{sp} = \frac{N_U \cdot k_B \cdot T}{2} \left\{ \begin{aligned} & \left[ (1-n-p) - 2 \cdot T \cdot \frac{dp}{dT} \right] \cdot \left[ \frac{4}{1-n-p} + \frac{n+p}{n \cdot p} \right] \cdot \frac{dp}{dT} + \left[ 4 + \frac{(1-n-p) \cdot (n+p)}{n \cdot p} \right] \cdot \left[ \frac{dp}{dT} + T \cdot \frac{d^2p}{dT^2} \right] \\ & + \left[ 4 \cdot \frac{dp}{dT} + 2 \cdot T \cdot \frac{d^2p}{dT^2} \right] \cdot \ln \left[ \frac{(1-n-p)^2}{n \cdot p} \right] + \left[ \frac{2 \cdot (1-2 \cdot n-2 \cdot p)}{n \cdot p} - \frac{(1-n-p) \cdot (n+p)}{n^2 \cdot p^2} \right] \cdot T \cdot \left( \frac{dp}{dT} \right)^2 \end{aligned} \right\} \quad (12)$$

There are two unknown parameters implicit in Equation (12):  $\Delta U$  and  $\Delta S$ . These must be determined by fitting to experimental data, e.g. the enthalpy measurements of Hein and Flagella (Reference [9]), after subtracting the contributions to the enthalpy due to the effects of harmonic and anharmonic vibration, lattice dilation and Schottky defects. These two parameters ( $\Delta U$  and  $\Delta S$ ) can also be determined by fitting to experimental data on the electrical conductivity of  $UO_{2+x}$ . Winter has shown that  $\sigma$ , the electrical conductivity of  $UO_{2+x}$ , can be described by the following:

$$\sigma = \frac{C_\sigma}{T} \cdot \left( \frac{e}{k_B} \right)^2 \cdot (n+p) \cdot (1-n-p) \cdot e^{\Delta E / (k_B \cdot T)} \quad (13)$$

where:

- $C_\sigma$  is a constant;  $C_\sigma = \frac{4 \cdot v \cdot k_B}{a_0}$  [W/(m·K)]
- $e$  is the electron charge [ $1.6021892 \cdot 10^{-19}$  C]
- $\Delta E$  is the electron mobility activation energy [J]
- $v$  is related to the electron jump frequency,  $\omega$ , via  $\omega = v \cdot \exp(-E / (k \cdot T))$  [1/s]
- $a_0$  is the lattice constant [m]

The unknown parameters in Equation (13) are  $\Delta U$ ,  $\Delta S$ ,  $\Delta E$  and  $C_\sigma$ . Winter proposes values for these parameters of  $\Delta U=2$  eV,  $\Delta S=2 \cdot k_B$ ,  $\Delta E=0.3$  eV and  $C_\sigma=2.83$  W/(m·K). These data allow the predicted electrical conductivities to exactly match the experimentally-derived correlation defined by Aronson (Reference [12]). However, these values do not provide an acceptable fit to the electrical conductivity data of Killeen (Reference [13]) at  $x=0.005$ , nor to the enthalpy data of Hein and Flagella ( $x=0.003$ ). However, using the values of the parameters from Winter's paper as a starting point, a set of four values can be found which results in predictions that agree with all three published works within their experimental uncertainties. In order to do this, numerically-determined best fits to each separate data set were first found and then values within the range of these variables were selected such that the agreement to Aronson's, Killeen's and Hein & Flagella's data were all equally good. The resulting values are  $\Delta U=4.33 \cdot 10^{-19}$  J (2.7 eV),  $\Delta S=2.62 \cdot 10^{-23}$  J/K ( $1.9 \cdot k_B$ ),  $\Delta E=4.81 \cdot 10^{-20}$  J (0.3 eV) and  $C_\sigma=3.71$  W/(m·K)

Figure 3 shows a comparison between the experimentally-based excess enthalpy and the enthalpy contribution from the integral of Equation (12) using  $\Delta U=4.33 \cdot 10^{-19}$  J and  $\Delta S=2.62 \cdot 10^{-23}$  J/K. The graph shows the enthalpy due to small polaron excitation for the uncertainty in the stoichiometric deviation as quoted in Hein & Flagella's work ( $x=0.003 \pm 0.003$ ). Agreement is within the experimental error.

Figure 2 shows the impact of the small polaron contribution to enthalpy (the integral of Equation (12)) on the agreement between experimental heat enthalpy data due to Hein and Flagella (Reference [9]) and the enthalpy determined based on the integral of the heat capacity model. Addition of this contribution improves the agreement with the experimental data.

Figure 4 shows a 3-D surface plot of Equation ( 12 ) for a range of stoichiometric deviations and temperatures. The graph shows that stoichiometric deviation can have a significant impact on this component of the heat capacity. Functionally,  $C_v^{sp}(x, T) = C_v^{sp}(-x, T)$ . Note that the values plotted for temperatures above the melting point are only of academic interest, since this model assumes that the U sub-lattice is present to interact with the hopping electrons. Once the fuel has melted, this would of course not be true and Equation ( 12 ) would no longer apply.

Hence, the heat capacity of  $UO_{2\pm x}$  due to lattice vibration, lattice dilation, Schottky defects and small polarons is:

$$C_p = 3 \cdot N(x) \cdot k_B \cdot \left[ \frac{1}{3+x} \cdot \left( \frac{3 \cdot T^3}{\Theta_D^3} \right) \cdot \int_0^{\Theta_D/T} \frac{z^4 \cdot e^z}{(e^z - 1)^2} dz + \frac{2+x}{3+x} \cdot \left( \frac{\Theta_E}{T} \right)^2 \cdot \frac{e^{\Theta_E/T}}{(e^{\Theta_E/T} - 1)^2} \right] + C_{anh} \cdot T + C_{sch} \cdot T$$

$$+ \frac{C_{dl} \cdot T + C_{d2} \cdot T^2}{1-P} + \frac{N_U \cdot k_B \cdot T}{2} \left\{ \begin{array}{l} \left[ (1-n-p) - 2 \cdot T \cdot \frac{dp}{dT} \right] \cdot \left[ \frac{4}{1-n-p} + \frac{n+p}{n \cdot p} \right] \cdot \frac{dp}{dT} \\ + \left[ 4 \cdot \frac{dp}{dT} + 2 \cdot T \cdot \frac{d^2p}{dT^2} \right] \cdot \ln \left[ \frac{(1-n-p)^2}{n \cdot p} \right] \\ + \left[ 4 + \frac{(1-n-p) \cdot (n+p)}{n \cdot p} \right] \cdot \left[ \frac{dp}{dT} + T \cdot \frac{d^2p}{dT^2} \right] \\ + \left[ \frac{2 \cdot (1-2 \cdot n-2 \cdot p)}{n \cdot p} - \frac{(1-n-p) \cdot (n+p)}{n^2 \cdot p^2} \right] \cdot T \cdot \left( \frac{dp}{dT} \right)^2 \end{array} \right\} \quad (14)$$

*Heat Capacity of  $UO_{2\pm x}$  for  $2670 K < T < T_{melt}$*

In 1968, Bredig predicted that  $UO_2$  should undergo an order-disorder transition (see Reference [14]), *i.e.* a cooperative process resulting in a loss of the long range order of the Oxygen ions on the  $UO_2$  lattice. The transition was predicted to be of second order (*i.e.* a  $\lambda$  transition). In the case of  $UO_2$ , it is usually referred to as the "Bredig transition" and has been experimentally determined to occur at 2670 K in unirradiated, stoichiometric  $UO_2$  (Reference [15]). The Bredig transition is associated with a "peak" in the heat capacity, in which the heat capacity appears to diverge, which is typical of such phase changes. However, this peak is very narrow in width, and the energy associated with the transition is relatively small. Therefore, the energy associated with this peak is ignored in this model. Additionally, since irradiation tends to favour transitions to a more disordered state, the peak is also likely to be somewhat "blurred" for fuel which is in a neutron flux.

Figure 5 shows the experimental enthalpy data from Hein and Flagella in the temperature range above this transition, along with the integral of Equation ( 14 ). Above the transition temperature of 2670 K, the heat capacity appears to be constant. The small polaron contribution to the heat capacity should be approximately constant in this temperature range for the given stoichiometric deviation. Equation ( 14 ) does yield an approximately constant heat capacity in this temperature regime, but its value is too low to be in agreement with the experimental data.

Since the Bredig transition does not affect the U sub-lattice, the small polaron contribution to the heat capacity should still exist in this temperature regime. Therefore, the small polaron contribution to the heat capacity is still applicable "unmodified", for temperatures between the Bredig transition and the melting point. The balance of the heat capacity in this temperature regime is of unknown functional form. If the small polaron contribution to the enthalpy is subtracted from Hein and Flagella's data and a linear best fit is made, an empirical heat capacity due to all other potential contributors can be determined. The value of this heat capacity component is equal to the slope of the best fit line (556.8 J/(kg·K)). Hence the heat capacity in this temperature range is modelled by:

$$C_p \Big|_{T>2670} = C_v^{sp} + 556.8 \text{ J/(kg·K)} \quad (15)$$

Figure 5 shows a comparison of the enthalpy data of Hein and Flagella in the temperature range between 2670 K and the melting point, along with the integrals of Equation ( 15 ) and Equation ( 14 ). The difference between the enthalpy data points and the integral of Equation ( 15 ) is due to the fact that the enthalpy associated with the peak in heat capacity at the Bredig transition temperature is not modelled. The difference is within the experimental uncertainty in the data, however, and so any estimate of the enthalpy associated with the peak would be highly uncertain.

Non-stoichiometry could potentially have an impact on the temperature at which the Bredig transition occurs. A theoretical treatment of this is given in Reference [4], which indicates that the Bredig transition temperature increases with the magnitude of the stoichiometric deviation, regardless of its sign. This prediction is verified by experimental evidence presented in the reference. Therefore, for non-stoichiometric  $UO_2$ , the increasing heat capacity due to lattice dilation, Schottky defects, and anharmonic vibrations will presumably continue to higher temperatures. It is difficult to quantify the magnitude of the change in the Bredig transition temperature with stoichiometric deviation, however, so it will be assumed for this model that the temperature of the Bredig transition remains unchanged for  $UO_{2\pm x}$ .

#### *Latent Heat of Fusion of $UO_{2\pm x}$*

For near-stoichiometric  $UO_2$  ( $x = 0.003 \pm 0.003$ ), Hein and Flagella's enthalpy measurements (see Reference [9]) can be used to determine the magnitude of the latent heat of fusion. Figure 6 shows the enthalpy data from this reference. The increase in enthalpy at the point of melting is clear. The figure shows that the latent heat of melting of nominally stoichiometric  $UO_2$  is  $282.184 \pm 9.472$  kJ/kg. For this model, it is assumed that deviations from stoichiometry and burnup in the range characteristic of CANDU (< at%) have a negligible effect on the magnitude of the latent heat of fusion.

#### *$C_p$ of Molten $UO_{2\pm x}$*

There is very little experimental data on the heat capacity of molten  $UO_2$ . Aside from the data of Ronchi *et. al.* (Reference [16]), there are only 10 experimental data points from two other experiments (References [9] and [17]) covering the temperature range from 3141 K to 3558 K. The scatter of these data is sufficiently high with respect to the temperature range covered that it is impossible to determine even the sign of  $dC_p/dT$ . Therefore, the data from Reference [16] is used for the development of the model for heat capacity of molten  $UO_2$ .

Along with the experimental data, Reference [16] provides a functional best fit to the experimental data which, while closely reproducing a fourth-order polynomial best fit to the data, formally represents the descending flank of a thermally activated specific heat contribution, plus another thermally activated term which is not significant until temperatures >4500-5000 K are achieved. The functional form of the expression for heat capacity of molten, stoichiometric  $UO_2$  is:

$$C_p \Big|_{T > T_{\text{melt}}} = 3 \cdot N \cdot k_B + \frac{1.1 \cdot 10^7}{T^2} \cdot e^{15500/T} + \frac{1.0 \cdot 10^{12}}{T^2} \cdot e^{-35500/T} \quad (16)$$

Figure 7 shows the heat capacity data compared to the above expression. Agreement is well within the experimental error.

Hyper- and hypo-stoichiometric  $UO_2$  do not melt congruently. Therefore, it is not physically accurate to speak of temperatures below or above the melting point with non-stoichiometric fuel. It is only appropriate to speak of material at a specific temperature with a specific mass fraction being solid (or a specific mass fraction liquid). The overall heat capacity will be the mass-weighted average of the heat capacities of the solid and liquid fractions. As fuel burnup ( $\omega$ ) increases, the addition of fission product "impurities" causes the solidus temperature to decrease, analogous to the effect of stoichiometric variations.

The expression for the heat capacity of liquid  $UO_2$  has three terms:

- 1) The Dulong-Petit heat capacity, due to atomic vibration,  $3 \cdot N \cdot k_B$
- 2) A term which represents the reduction in  $C_p$  due to the saturation of the additional thermally-activated processes which are important for solid phase fuel,  $1.1 \cdot 10^8 / T^2 \cdot e^{15500/T}$
- 3) A term which represents excitation of electrons in the 2p orbitals,  $1.0 \cdot 10^{12} / T^2 \cdot e^{-35500/T}$

The first term will be altered by non-stoichiometry as described by the first term of Equation ( 6 ). Hence, this term becomes  $3 \cdot N(x) \cdot k_B$ .

The reduction in heat capacity described by the second term in equation (16) is associated with the melting process. The term must be "corrected", therefore, so that the reduction is consistent for cases in which the amounts by which the actual temperature exceeds the liquidus temperature are the same.

The third term in equation (16) is not driven by the melting process. It represents excitation of electrons between orbitals, and so should be, in principle, affected by the presence of additional O atoms. However, since the orbitals in question (2p) are relatively deep in the electron structure of U, the impact is assumed to be negligible.

Therefore, the expression for the heat capacity of irradiated liquid  $UO_{2+x}$  is:

$$C_p \Big|_{T > T_L(x, \omega)} = 3 \cdot N(x) \cdot k_B + \frac{1.1 \cdot 10^7}{T'(x, \omega)^2} \cdot e^{15500/T'(x, \omega)} + \frac{1.0 \cdot 10^{12}}{T^2} \cdot e^{-35500/T} \quad (17)$$

where:

$T'(x, \omega)$  is defined as  $T_L(0, 0) + \{T - T_L(x, \omega)\}$  [K]

$T_L(x, \omega)$  is the liquidus temperature for the fuel as a function of stoichiometric deviation and burnup [K]

#### *Overall Model of Fuel Heat Capacity*

The fuel heat capacity model consists of three different models for different temperature ranges. For temperatures up to 2670 K, Equation ( 14 ) applies. For solid urania above 2670 K, Equation ( 15 ) applies. For liquid urania, Equation ( 17 ) applies. For mixed phase situation, the mass-weighted average of the heat capacities for solid and liquid are used. Figure 1 plots the overall model of fuel heat capacity as a function of temperature for various values of the stoichiometric deviation, porosity and burnup.

#### **Thermal Conductivity of $UO_{2+x}$**

Thermal conductivity is a measure of the "ease" of internal transfer of energy between regions of a material. This energy can be transferred through the following mechanisms:

- 1) Lattice vibrations (phonons)
- 2) Electron-hole movement
- 3) Radiant heat transfer

#### *Phonon Contribution to Thermal Conductivity*

The thermal conductivity due to lattice vibrations (or phonons) can be expressed as the following:

$$k_p = \rho \cdot C_v^{latt} \cdot u \cdot \frac{\lambda}{3} \quad (18)$$

where:

- $k_p$  is the contribution to thermal conductivity due to phonons, [W/(m·K)]. Note that, below 1500 K,  $k \approx k_p$
- $\rho$  is the density [10960 kg/m<sup>3</sup> for 100% TD  $UO_2$ ]
- $C_v^{latt}$  is the phonon contribution to the specific heat at constant volume [J/(kg·K)]
- $u$  is the mean phonon speed [m/s]
- $\lambda$  is the phonon mean free path [m]

The density can be determined using a fuel thermal expansion correlation such as is found in Reference [18].

For application in this context, the above expression should only be used in the case of solid urania. If the material is liquid, there will still be atomic vibrations, but they will not propagate spatially due to the lack of a rigid atomic lattice. Therefore, for liquid  $\text{UO}_2$ ,  $k_p = 0$ .

Unfortunately, the expression  $v \cdot \lambda / 3$  consists of two parameters which cannot be determined via direct measurement. However, this expression is dominated by two main contributions for temperatures below 3000 K (Reference [18]). These contributions are the deflection or scattering of phonons from lattice defects, and phonon self-scattering. These processes are functions of the stoichiometric deviation of the fuel and its impurity content. With the assumption that these two processes dominate the phonon mean free path, Equation ( 18 ) becomes:

$$k_p = \frac{\rho \cdot C_v^{\text{latt}}}{A(x, \omega) + B(x, \omega) \cdot T'} \quad (19)$$

where:

- $A(x, \omega)$  is a factor proportional to the point defect contribution to the phonon mean free path [m·s/kg]
- $B(x, \omega)$  is a factor proportional to the phonon-phonon scattering contribution to the mean free path [m·s/(kg·K)]
- $T'$  is the temperature or 2050 K, whichever is less [K]

The factors  $A(x, \omega)$  and  $B(x, \omega)$  are determined by deriving correlations to thermal conductivity data. See below for details of their derivation.  $T'$  is used in this equation instead of  $T$  because, at 2050 K, the mean free path of the phonons becomes about equal to the inter-atomic distance. Therefore, following Reference [18], the temperature used is limited to this value.

Equation ( 19 ) gives the expression for non-porous material. In reality,  $\text{UO}_2$  is porous. Pores have a different thermal conductivity than the  $\text{UO}_2$  lattice and this must be accounted for. This is done using either the modified Loeb equation or the Maxwell-Eucken equation. The Maxwell-Eucken equation is considered to be superior to the modified Loeb equation (Reference [19]) and is used in this model. The Maxwell-Eucken equation is as follows:

$$\frac{k_p}{k_{100}} = \frac{1 - P}{1 + \beta \cdot P} \quad (20)$$

where:

- $k_p$  is the thermal conductivity due to phonons in porous material [W/(m·K)]
- $k_{100}$  is the thermal conductivity in a sample of the material with no pores [W/m·K] (see Equation ( 19 ))
- $\beta$  is a factor which depends on the shape, distribution and composition of the pores

The thermal conductivity of  $\text{UO}_2$  is commonly measured indirectly. This is done by measuring the thermal diffusivity,  $\alpha$ :

$$\alpha = \frac{k}{\rho \cdot C_p} \quad (21)$$

where:

- $k$  is the thermal conductivity [W/(m·K)]
- $C_p$  is the heat capacity [J/(kg·K)]

For  $T < 1773$  K,  $k \approx k_p$  and  $C_p \approx C_v^{\text{latt}}$ . Using this fact and Equations ( 19 ) and ( 20 ), it is easy to show that the thermal diffusivity in this temperature regime can be expressed by:

$$\alpha = \left( \frac{1 - P}{1 + \beta \cdot P} \right) \cdot \frac{1}{A(x, \omega) + B(x, \omega) \cdot T} \quad (22)$$

As mentioned in above, this model uses a correlation to determine the value of  $\beta$ . In order for the correlation to be applicable to CANDU nuclear fuel, the experimental data on which the correlation is based must be for fuel as similar as possible to CANDU fuel. For this reason, SIMFUEL data from Reference [20] is selected as the basis for determining the experimental constants in Equation ( 22 ). This model will follow Reference [18] and use an expression for  $\beta$  of the form:

$$\beta = \beta_1 + \beta_2 \cdot T \quad (23)$$

Due to the nature of the variation of  $\beta(T)$  with  $T$ , this correlation implies that  $\beta(T)$  will eventually become less than -1 as the temperature increases. This leads to the implication that, above a certain temperature, fuel with porosity has a higher thermal conductivity than  $\text{UO}_2$  at 100% TD. Reference [18] deals with this by using a "cutoff" temperature beyond which  $\beta$  is held constant at a value of -1, with a linear interpolation over a limited temperature range around this cutoff.

In order to determine the functional form of  $A(x,\omega)$  and  $B(x,\omega)$ , the values of  $A$  and  $B$  for a range of stoichiometric deviations and simulated burnups from Reference [20] were used as the starting point. The values of  $A$  and  $B$  in Reference [20] are peculiar to the assumptions and measurements made in Reference [20], so they are not simply used in this model. Instead, the values of  $A$  and  $B$  from Reference [20] will be used to determine the appropriate functional form of the expressions for  $A(x,\omega)$  and  $B(x,\omega)$ , and then the coefficients of the functions will be determined so as to be consistent with all of the elements of this model. Table 1 and Table 2 reproduce the values of  $A$  and  $B$  reported in Reference [20]. If the data for  $A$  are graphed, and a term of the form  $A_1 + A_2 \cdot x$  is removed from them, what is left appears to follow a power law relationship, linear in  $x$  and  $\omega$ . Hence, a valid empirical expression for  $A(x,\omega)$  is:

$$A(x,\omega) = A_1 + A_2 \cdot x + 10^{A_3 + A_4 \cdot \omega + A_5 \cdot x} \quad (24)$$

If the data for  $B$  are plotted, it can be seen that the dependence on  $x$  and  $\omega$  does not appear to be strong and there is a good deal of "scatter" in the relationship. However, there does seem to be some dependence, so it is assumed that  $x$  and  $\omega$  result in a first-order correction to the value of  $B$ , leading to the following empirical expression for  $B(x,\omega)$ :

$$B(x,\omega) = B_1 + B_2 \cdot \omega + B_3 \cdot x \quad (25)$$

With these functional forms for  $\beta(T)$ ,  $A(x,\omega)$  and  $B(x,\omega)$ , an iterative technique was used to determine the best fit values of  $\beta_1$ ,  $\beta_2$ ,  $A_1$ ,  $A_2$ ,  $A_3$ ,  $A_4$ ,  $A_5$ ,  $B_1$ ,  $B_2$  and  $B_3$  using the data from Reference [20]. The initial values of  $\beta_1$  and  $\beta_2$  are from Reference [18] and the initial values of the other eight unknowns are the best fit values for the values of  $A$  and  $B$  in Table 1 and Table 2. The experimental data consist of 136 measurements covering stoichiometric deviations from 0.0 - 0.084, simulated burnups from 0 - 1800 MW·h/kgU (*cf.* usual CANDU average exit burnup: ~190 MW·h/kgU) and densities from 10.512 - 10.776 g/cm<sup>3</sup> (*cf.* CANDU  $\text{UO}_2$  density specification: 10.45 - 10.75 g/cm<sup>3</sup>).

An additional constraint was placed on the solution. Recall that Equation ( 23 ) is not applied at all temperatures. Above the "cutoff" temperature, the value of  $T$  used in Equation ( 23 ) is the "cutoff" temperature. In Reference [18], the "cutoff" temperature is near 1773 K. The data in Reference [20] show a tendency for higher densities to result in higher thermal conductivities even up to 1773 K, implying that the cutoff temperature is some temperature  $\geq 1773$  K.

If the "cutoff" temperature were to be in the temperature range of the experimental data used to derive the values of the coefficients for  $\beta(T)$ ,  $A(x,\omega)$  and  $B(x,\omega)$ , it would greatly complicate the solution process, due to the non-linearity which would be introduced. Therefore, in order to make the numerical solution process more tractable, a constraint was added to the numerical solution that the "cutoff" temperature had to be  $\geq 1773$  K. The values of the fitting parameters with this constraint are given in Table 3. The "cutoff" temperature implied by the values of  $\beta_1$  and  $\beta_2$  is 1773 K.

The standard error of the fit to the data with the values of the fitting parameters given in Table 3 is 4.3%, which is similar to the quoted experimental error for the data of 5%. The maximum error for any particular data point is 10.4%. Figure 8 shows a plot of predicted vs. measured thermal diffusivities using the best fit values of the fitting parameters. Agreement is excellent. Confirmation that the deviations between the model predictions and the experimental data can be ascribed to random error is found in Figure 9, which compares the distribution of the relative errors in the predictions with the normal distribution. A  $\chi^2$  test shows that the difference between the actual error distribution and the normal distribution is not statistically significant.

This error analysis demonstrates that the correlations derived for  $\beta$ , A and B are sufficiently close to the "true" relationships that the differences between model prediction and the experimental data in Reference [20] can be ascribed to stochastic processes. This conclusion lends support to extrapolation of the correlations for A and B beyond the ranges of stoichiometric deviation and density for which they were derived, so long as the structure of the material is still  $\text{UO}_{2\pm x}$ .

The derivation of correlations above has been restricted to fuel which is either nominally stoichiometric or hyper-stoichiometric. It is important to also consider hypo-stoichiometric fuel.  $\beta$  is not dependent on stoichiometric deviation, so application of the relation for  $\beta(T)$  is not restricted to hyper-stoichiometric fuel. A and B, however, are dependent on stoichiometric deviation and their behaviour in this regime must be assessed.

The stoichiometric deviation affects A and B because of the presence of lattice defects. In  $\text{UO}_{2+x}$ , the defects are interstitial O ions; in  $\text{UO}_{2-x}$ , they are O vacancies (Reference [21]). In either case (*i.e.* hyper- or hypo-stoichiometric fuel), the molar density of defects is the same and so, the number and distribution of "order defects" is the same. The assumption is therefore made that  $A(x, \omega) = A(-x, \omega)$  and  $B(x, \omega) = B(-x, \omega)$ . This alters the functional form for A and B slightly:

$$A(x, \omega) = A_1 + A_2 \cdot |x| + 10^{A_3 + A_4 \cdot \omega + A_5 \cdot |x|} \quad (26)$$

$$B(x, \omega) = B_1 + B_2 \cdot \omega + B_3 \cdot |x| \quad (27)$$

This modification allows the expression for  $k_p$  to be applied to hypo-stoichiometric fuel.

If the assumptions underlying Equations ( 26 ) and ( 27 ) are reasonable, one would expect that, as long as the stoichiometric deviation is above the  $[\text{U} + \text{UO}_{2-x}]$  phase boundary, the thermal conductivity of hypo-stoichiometric urania would be similar to the thermal conductivity of hyper-stoichiometric urania whose stoichiometric deviation was of the same magnitude. Reference [22] shows the experimental results of Hetzler, which were performed for urania with an O/U ratio of 1.98 and 1.97 (*i.e.*  $x = -0.02$  and  $x = -0.03$ ) and compares them to the results of Howard, Ross and Belle for slightly hyper-stoichiometric  $\text{UO}_{2+x}$  with  $x$  in the range between 0 and 0.18. The results show that, below a certain threshold temperature which appears to be close to the  $[\text{U} + \text{UO}_{2-x}]$  phase boundary, the thermal conductivity of hypo-stoichiometric urania is much higher than that of similarly hyper-stoichiometric material. However, above this temperature (*i.e.* in the  $\text{UO}_{2-x}$  phase), the thermal conductivity falls to a value near that observed in hyper-stoichiometric urania. This indicates that the conceptual model underlying the extension of Equations ( 24 ) and ( 25 ) to the forms shown in Equations ( 26 ) and ( 27 ) is a reasonable one.

#### *Small Polaron Contribution to Thermal Conductivity*

The second significant contributor to the thermal conductivity of  $\text{UO}_{2\pm x}$  fuel is electron-hole transport. Some treatments of thermal conductivity of urania use an expression for this contribution to the thermal conductivity which assumes that the fuel behaves as a semiconductor. However, as discussed above, urania is a Mott insulator, rather than a semiconductor. Thus there is no Weidmann-Franz term as is the case for semiconductors. This yields an expression for the thermal conductivity due to electron-hole transport of:

$$k_e = \left( \frac{k_B}{e} \right)^2 \cdot T \cdot \frac{\sigma_e \cdot \sigma_h}{\sigma_e + \sigma_h} \cdot \left( \frac{\Delta U}{k_B \cdot T} \right)^2 \quad (28)$$

where:

- $k_e$  is the thermal conductivity due to electron-hole transport [W/(m·K)]
- $\sigma_e$  is the partial dc electric conductivity due to electron transport [1/(Ω·m)]
- $\sigma_h$  is the partial dc electric conductivity due to hole transport [1/(Ω·m)]

Reference [11] provides a theoretical technique for evaluating the above expression for a given temperature and stoichiometric deviation,  $x$ . This treatment results in the following expression for this component of the thermal conductivity of  $UO_{2+x}$ :

$$k_e = C_\sigma \cdot \left( \frac{\Delta U}{k_B \cdot T} \right)^2 \cdot \frac{n \cdot p \cdot (1 - n - p)}{n + p} \cdot e^{-\Delta E / (k_B \cdot T)} \quad (29)$$

where:

- $C_\sigma$  is a constant;  $C_\sigma = \frac{4 \cdot v \cdot k_B}{a_o}$  [W/(m·K)]
- $v$  is related to the electron jump frequency,  $\omega$ , via  $\omega = v \cdot \exp(-E / (k_B \cdot T))$  [1/s]
- $a_o$  is the lattice constant [m]

Note that the above expressions for  $k_e$  are only valid for solid phase urania. For liquid material, the “hopping” mode of electron and hole transport would not occur, since there would not be a U cation sub-lattice in place to provide the lattice polarisations. However, this would imply that electrons produced would be *more* mobile than if the U sub-lattice were there. Therefore, applying the above formulation to the determination of  $k_e$  in liquid urania should result in an under-prediction, allowing for conservative (from the point of view of fission product release) over-estimates of fuel temperature.

The values of the parameters  $C_\sigma$ ,  $\Delta U$ ,  $\Delta S$  and  $\Delta E$  used in the thermal conductivity model are identical to those used for the heat capacity model described above.

#### *Radiative Contribution to Thermal Conductivity*

The final contributor to the thermal conductivity is radiative heat transport.  $UO_2$  will have a contribution to thermal conductivity which is of the following form (see Reference [23]):

$$k_{\text{rad}} = \frac{16}{3} \cdot \left[ \frac{\sigma_s}{\alpha_s(\lambda, T)} \right] \cdot N^2(\lambda, T) \cdot T^3 \quad (30)$$

where:

- $\sigma_s$  is the Stefan-Boltzmann constant
- $\alpha_s(\lambda, T)$  is the spectral absorption coefficient
- $N(\lambda, T)$  is the index of refraction

The typical approach is to assume that  $N(\lambda, T)$  is independent of temperature and wavelength, and to average  $\alpha_s$  over the Planck distribution of the radiation to obtain a Rosseland absorption coefficient (temperature dependent only;  $\alpha_R(T)$ ), yielding the following expression for  $k_{\text{rad}}$ :

$$k_{\text{rad}} = 3 \cdot 10^{-11} \cdot \left[ \frac{N^2}{\alpha_R(T)} \right] \cdot T^3 \quad (31)$$

Hyland (Reference [23]) reports that the assumption that  $N$  is independent of  $\lambda$  and  $T$  is justified, based on the directional spherical reflectivity data of Bober *et al.* (Reference [24]), and that the value of  $N$  is 2.25. Experimental

data on  $\alpha_R(T)$  is highly uncertain, especially in the high temperature regime in which the radiative component of the thermal conductivity is important. Hyland has defined a lower bound on the possible values of  $\alpha_R(T)$ , which will be referred to as  $\alpha_R^{\min}(T)$  (see Table 4). This set of data lead to the indicated upper bound values of  $k_{\text{rad}}$ . However, because of uncertainties in the values of  $\alpha(\lambda, T)$  beyond the absorption edge of the material, the values of  $\alpha_R^{\min}(T)$  in Table 4 have an uncertainty band of +1000% and -0%. Another way of putting this is that the best estimate of  $k_{\text{rad}}$  is 1/2 of the value which would be obtained from the values of  $\alpha_R^{\min}(T)$  in Table 4, with an uncertainty of  $\pm 100\%$ . This leads to the following expression for  $k_{\text{rad}}$ :

$$k_{\text{rad}} = \frac{3 \cdot 10^{-11}}{2} \cdot \left[ \frac{N^2}{\alpha_R^{\min}(T)} \right] \cdot T^3 \quad (32)$$

The data for  $\alpha_R(T)$  in Table 4 can be easily fit to a power law. The best fit expression for the data is:

$$\alpha_R^{\min}(T) = C_1 \cdot \exp(C_2 \cdot T) \quad (33)$$

where:

- $C_1$  has a value of  $8750 \text{ m}^{-1}$   
 $C_2$  has a value of  $7.5971 \cdot 10^{-4} \text{ K}^{-1}$

The resulting expression for  $k_{\text{rad}}$  has an uncertainty of  $\pm 100\%$ . However, the theoretical basis is sound and the contribution of  $k_{\text{rad}}$  to the overall thermal conductivity is not dominant. Therefore, the effect is included in this model for thermal conductivity. Since this contribution to the thermal conductivity is related to the behaviour of photons in the fuel, it should not be significantly affected by changes in stoichiometric deviation or by burnup. Any such effect is assumed to be insignificant in this model.

#### *Effect of In-Reactor Flux on Thermal Conductivity*

When the urania is in the reactor, the flux will have an effect on the thermal conductivity. Damage to the lattice structure of the fuel (e.g. dislocations) will interfere with the propagation of phonons, reducing the thermal conductivity. However, annealing of these lattice defects will act to negate this effect, so that at high temperatures the effect of being in flux is negligible. Reference [22] shows the results of Clough and Sayers (Reference [25]), who determined the thermal conductivity of  $\text{UO}_2$ . These results clearly demonstrate that the thermal conductivity of  $\text{UO}_2$  under irradiation can be broken into three regimes:

- 1)  $T > 773 \text{ K}$ : the thermal conductivities of unirradiated fuel and fuel undergoing irradiation are the same.
- 2)  $523 \text{ K} \geq T \geq 773 \text{ K}$ : the thermal conductivity of fuel undergoing irradiation is approximately constant, while the thermal conductivity of unirradiated fuel increases with decreasing temperature.
- 3)  $T < 523 \text{ K}$ , the thermal conductivity curve is very similar to the curve for unirradiated fuel at temperatures  $\sim 150 \text{ K}$  higher.

This model adopts a very simple expedient to account for the effect of in-reactor flux on fuel thermal conductivity. For temperatures below  $773 \text{ K}$ , the thermal conductivity at  $773 \text{ K}$  will be used. This ignores the observed trend on thermal conductivity at temperature below  $523 \text{ K}$ , but such temperatures are of little interest in safety analysis and the under-prediction implicit in this model's approach is considered to be acceptable.

#### *Effect of Mixed Solid and Liquid Phase on Thermal Conductivity*

Non-stoichiometric urania has separate solidus and liquidus temperatures. Because of this, it is possible to have states in which a urania sample may be of mixed phase; i.e. the sample may contain both solid and liquid material at a constant temperature.

In this event, the thermal conductivity of mixed phase urania will be determined based on the approach described in Reference [26].

To apply this approach, the thermal conductivities of both the solid and liquid phases in the fuel are determined. Next the phase whose volume fraction is >50% is labelled as the continuous phase; the other phase is labelled the dispersed phase. If the solid urania is the continuous phase, the effective thermal conductivity is given by:

$$k_{\text{eff}} = \left[ \frac{2}{\sqrt{-C' \cdot (k_d - k_c) \cdot [k_c + B \cdot (k_d - k_c)]}} \cdot \tan^{-1} \left\{ \frac{B}{2} \cdot \sqrt{\frac{C' \cdot (k_d - k_c)}{k_c + B \cdot (k_d - k_c)}} \right\} + \frac{1-B}{k_c} \right]^{-1} \quad (34)$$

where:

- $k_{\text{eff}}$  is the effective thermal conductivity of the two-phase mixture (W/(m·K))  
 $k_c$  is the thermal conductivity of the continuous phase (W/(m·K))  
 $k_d$  is the thermal conductivity of the dispersed phase (W/(m·K))  
 $B = \sqrt{3 \cdot V_d / 2}$   
 $C' = 4 \cdot \sqrt{2 / (3 \cdot V_d)}$   
 $V_d$  is the volume fraction of the dispersed phase

If the liquid urania is the continuous phase, the effective thermal conductivity is given by:

$$k_{\text{eff}} = \left[ \frac{1}{\sqrt{C' \cdot (k_d - k_c) \cdot [k_c + B \cdot (k_d - k_c)]}} \cdot \ln \left\{ \frac{\sqrt{k_c + B \cdot (k_d - k_c)} + \frac{B}{2} \cdot \sqrt{C' \cdot (k_d - k_c)}}{\sqrt{k_c + B \cdot (k_d - k_c)} - \frac{B}{2} \cdot \sqrt{C' \cdot (k_d - k_c)}} \right\} + \frac{1-B}{k_c} \right]^{-1} \quad (35)$$

#### Overall Model for Fuel Thermal Conductivity

Based on the discussion in the above document, the thermal conductivity of a single-phase sample of Uranium dioxide fuel can be expressed by:

$$k = \left( \frac{1-P}{1+\beta \cdot P} \right) \cdot \frac{\rho \cdot C_v^{\text{latt}}}{A(x, \omega) + B(x, \omega) \cdot T} + C_\sigma \cdot \left( \frac{\Delta U}{k_B \cdot T} \right)^2 \cdot \frac{n \cdot p \cdot (1-n-p)}{n+p} \cdot e^{\Delta E / (k_B \cdot T)} + \frac{3 \cdot 10^{-11}}{2} \cdot \left[ \frac{N^2}{\alpha_{R \text{ min}}(T)} \right] \cdot T^3 \quad (36)$$

In the case of a mass of fuel which is of mixed solid and liquid phases, the above expression may be evaluated separately for the solid and liquid phases and Equations ( 34 ) and ( 35 ) used to determine the effective thermal conductivity of the overall mixture.

Equation ( 36 ) is plotted in Figure 10 as a function of temperature for various values of the stoichiometric deviation, porosity and burnup. Note that the effective thermal conductivity in the mixed solid/liquid phase region is not plotted.

#### References:

- 1 A.C. Brito, F.C. Iglesias, Y. Liu, C.J. Westbye, "Modelling of UO<sub>2</sub> Oxidation in Steam," presented at the 17th Annual Conference of the Canadian Nuclear Society, Fredericton, New Brunswick, Canada, June 9-12, 1996.
- 2 A.C. Brito, F.C. Iglesias, Y. Liu, M.A. Petrilli, M.J. Richards, R.A. Gibb & P.J. Reid, "SOURCE 2.0: A Computer Program to Calculate Fission Product Release From Multiple Fuel Elements for Accident Scenarios," presented at the 4th International Conference on CANDU Fuel, Pembroke, Ontario, October 1-4, 1995.
- 3 M.W. Zemansky & R.H. Dittman, "Heat and Thermodynamics: An Intermediate Textbook", 6<sup>th</sup> edition, McGraw-Hill Book Company, 1981
- 4 C. Ronchi & G.J. Hyland, "Analysis of Recent Measurements of the Heat Capacity of Uranium Dioxide", Journal of Alloys and Compounds 213/214 (1994) p. 159-168

- 5 B.T.M. Willis, Proceedings of the Royal Society of London **274** (1963) p. 134-144
- 6 IAEA, "Thermodynamic and Transport Properties of  $\text{UO}_2$  and Related Phases", Vienna: IAEA, (1965)
- 7 P. Browning, G.J. Hyland & J. Ralph, "The Origin of the Specific Heat Anomaly in Solid Urania", High Temperatures High Pressures **15** (1983) p. 169-178
- 8 J.L. Fink, M.G. Chasanov, L. Leibowitz, "Thermodynamic Properties of Uranium Dioxide", Argonne National Laboratory Report ANL-CEN-RSD-80-3, April 1981
- 9 R.A. Hein and P.N. Flagella, "Enthalpy Measurements of  $\text{UO}_2$  and Tungsten", GEMP-578, Presented at the 70<sup>th</sup> Annual Meeting of the American Ceramic Society, April 20-25, 1968. Chicago, Ill, USA, February 16, 1968
- 10 G.J. Hyland & J. Ralph, "Electronic Contributions to the High Temperature Thermophysical Properties of  $\text{UO}_{2+x}$ ", High Temperatures High Pressures **15** (1983) p. 179-190
- 11 P.W. Winter, "The Electronic Transport Properties of  $\text{UO}_2$ ", Journal of Nuclear Materials **161** (1989) p. 38-43
- 12 S. Aronson, J.E. Rulli & B.E. Schaner, "Electrical Properties of Nonstoichiometric Uranium Dioxide", Journal of Chemical Physics **35**
- 13 J.C. Killeen, "The Effect of Niobium Oxide Additions on the Electrical Conductivity of  $\text{UO}_2$ ", Journal of Nuclear Materials **88** (1980) p. 185-192
- 14 M.A. Bredig, "The Order-Disorder ( $\alpha$ - $\beta$ ) Transition in Uranium Dioxide and Other Solids of the Fluorite Type. Effect of Ion Size and Deviation from Stoichiometry", High-Temperature Thermochemistry section of "ORNL Chemistry Division Annual Progress Report for Period Ending May 20, 1969", ORNL-4437, September 1969
- 15 J.P. Hiernaut, G.J. Hyland & C. Ronchi, "Premelting Transition in Uranium Dioxide", International Journal of Thermophysics **14** no. 2 (1993) p. 259-283
- 16 C. Ronchi, J.P. Hiernaut, R. Salfslag & G.J. Hyland, "Laboratory Measurement of the Heat Capacity of Urania up to 8000 K: I. Experiment", Nuclear Science and Engineering **113** (1993) p. 1-19
- 17 L. Leibowitz, M.G. Chasanov, L.W. Mishler & D.F. Fischer, Journal of Nuclear Materials **140** (1986) p. 149
- 18 D.L. Hagrman, G.A. Reymann & R.E. Mason, "MATPRO-Version 11 (Revision 2): A Handbook of Materials Properties for Use in The Analysis of Light Water Reactor Fuel Behaviour", NUREG/CR-0497-REV 2, August 1981
- 19 G.P. Marino, "The Porosity Correction Factor for the Thermal Conductivity of Ceramic Fuels", Journal of Nuclear Materials **38**, 1971, pp. 178-190
- 20 P.G. Lucuta, H.J. Matzke & R.A. Verrall, "Thermal Conductivity of Hyperstoichiometric SIMFUEL", Journal of Nuclear Materials **223**, pp. 51-60, 1995
- 21 M.H. Rand, *et al.*, "The Thermodynamic Properties of the Urania Phase", Révue Internationale des Hautes Temperatures et des Réfactures **15**, pp. 355-365 1978
- 22 H. Marchandise, "Conductibilité Thermique du Bioxide d'Uranium", EUR-4568f, 1970
- 23 G.J. Hyland, "Thermal Conductivity of Solid  $\text{UO}_2$ : Critique and Recommendation", Journal of Nuclear Materials **113**, 1983, pp. 125-132
- 24 M. Bober, J. Singer & K. Wagner, Proceedings of the 8<sup>th</sup> Symposium on Thermophysical Properties, NBS Gaithersburg (1981)
- 25 D.J. Clough & J.B. Sayers, "The Measurement of the Thermal Conductivity of  $\text{UO}_2$  Under Irradiation in the Temperature Range 150-1600°C", AERE-R-4690 (1964)
- 26 S.C. Cheng & R.I. Vachon, "The Prediction of the Thermal Conductivity of Two and Three Phase Solid Heterogeneous Mixtures", International Journal of Heat and Mass Transfer **12**, pp. 249-264, 1969.

x (UO <sub>2+x</sub> )	A (m·K/W)		
	0 MW·h/kgU	675 MW·h/kgU	1800 MW·h/kgU
0.0000	0.0911	0.1362	0.1858
0.0069	0.1022	0.1433	—
0.0350	0.2031	0.1997	0.2345
0.0840	0.3669	0.3819	0.3844

Table 1: Value of Coefficient A in  $k = (A+B\cdot T)^{-1}$  from Reference [20]

x (UO <sub>2+x</sub> )	B (m/W)		
	0 MW·h/kgU	675 MW·h/kgU	1800 MW·h/kgU
0.0000	$2.35\cdot 10^{-4}$	$2.12\cdot 10^{-4}$	$2.05\cdot 10^{-4}$
0.0069	$2.33\cdot 10^{-4}$	$2.17\cdot 10^{-4}$	—
0.0350	$2.20\cdot 10^{-4}$	$2.23\cdot 10^{-4}$	$1.95\cdot 10^{-4}$
0.0840	$1.55\cdot 10^{-4}$	$1.34\cdot 10^{-4}$	$1.34\cdot 10^{-4}$

Table 2: Value of Coefficient B in  $k = (A+B\cdot T)^{-1}$  from Reference [20]

Constant	Initial Estimate	Final Value
$\beta_1$	6.5	5.74
$\beta_2$	-0.00469 K <sup>-1</sup>	-0.00380 K <sup>-1</sup>
$A_1$	255800 s/m <sup>2</sup>	-434000 s/m <sup>2</sup>
$A_2$	11607000 s/m <sup>2</sup>	8530000 s/m <sup>2</sup>
$A_3$	4.752	5.65
$A_4$	$4.62\cdot 10^{-4}$ kgU/(MW·h)	$1.09\cdot 10^{-4}$ kgU/(MW·h)
$A_5$	-15.955	-4.73
$B_1$	789 s/(m <sup>2</sup> ·K)	804 s/(m <sup>2</sup> ·K)
$B_2$	$-5.26\cdot 10^{-2}$ kgU·s/(m <sup>2</sup> ·K·MW·h)	$-3.96\cdot 10^{-2}$ kgU·s/(m <sup>2</sup> ·K·MW·h)
$B_3$	-3058 s/(m <sup>2</sup> ·K)	2150 s/(m <sup>2</sup> ·K)

Table 3: Initial Estimates and Best Fit Values of Unknown Constants in  $k_p$ 

Temperature (K)	$\alpha_R^{\min}(T)$ (cm <sup>-1</sup> )	Max. $k_{rad}$ (W/(m·K))	$k_{rad}$ (W/(m·K))
1000	190	0.08	$0.04 \pm 0.04$
2000	385	0.32	$0.16 \pm 0.16$
3000	865	0.47	$0.24 \pm 0.24$

Table 4: Lower Bound Values of  $\alpha_R(T)$  (after Reference [23]) and Corresponding Estimates of  $k_{rad}$

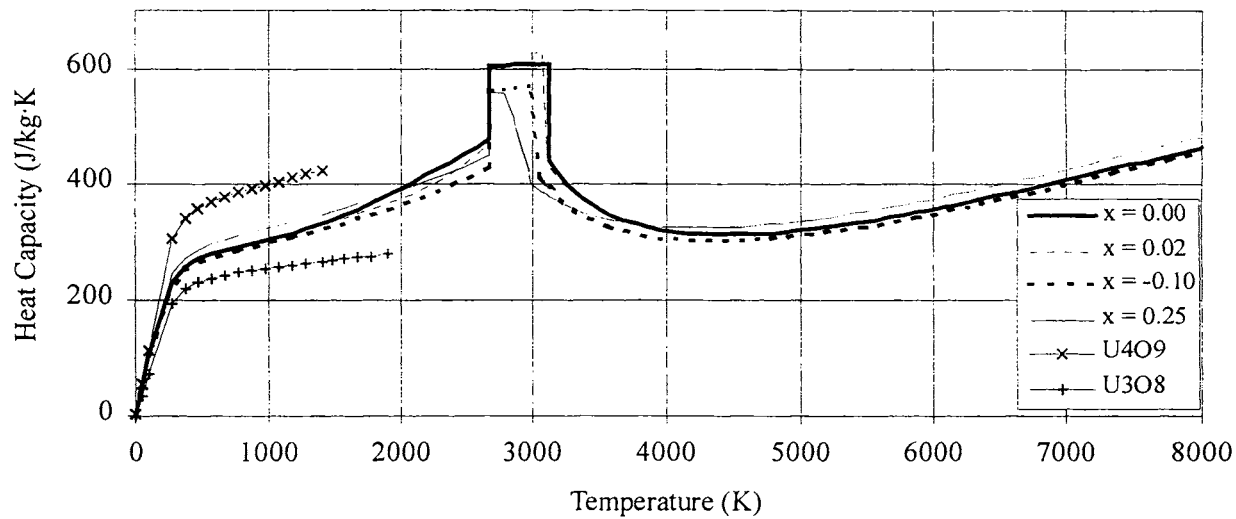


Figure 1: Overall Model of Heat Capacity of  $\text{UO}_{2+x}$  and Heat Capacity of  $\text{U}_4\text{O}_9$  and  $\text{U}_3\text{O}_8$

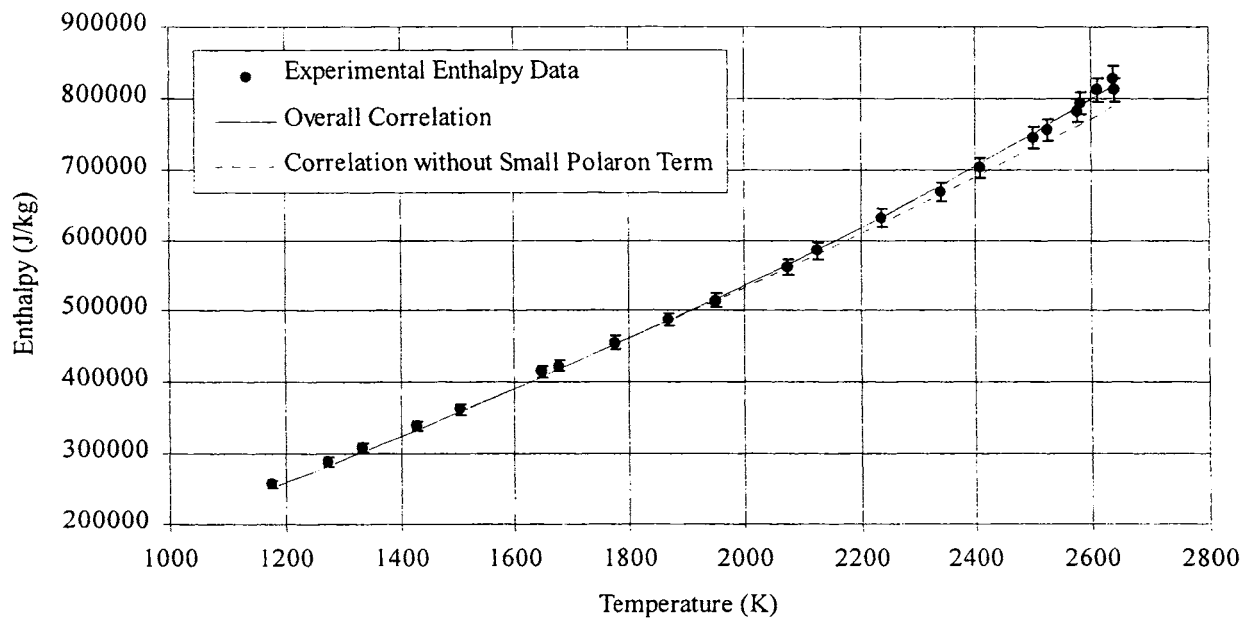


Figure 2: Enthalpy Data due to Hein & Flagella ( $x = 0.003 \pm 0.003$ ) and Heat Capacity Models With and Without Small Polaron Excitation

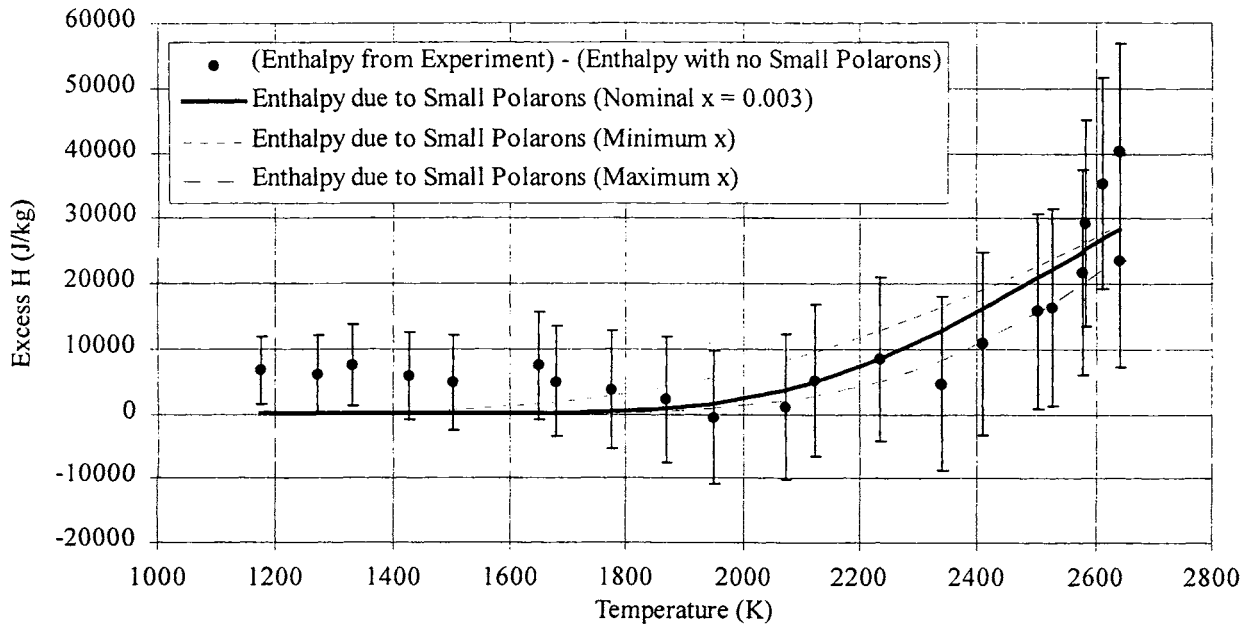


Figure 3: Comparison of Excess Experimental Enthalpy (Hein & Flagella) to Enthalpy due to Small Polaron Excitation

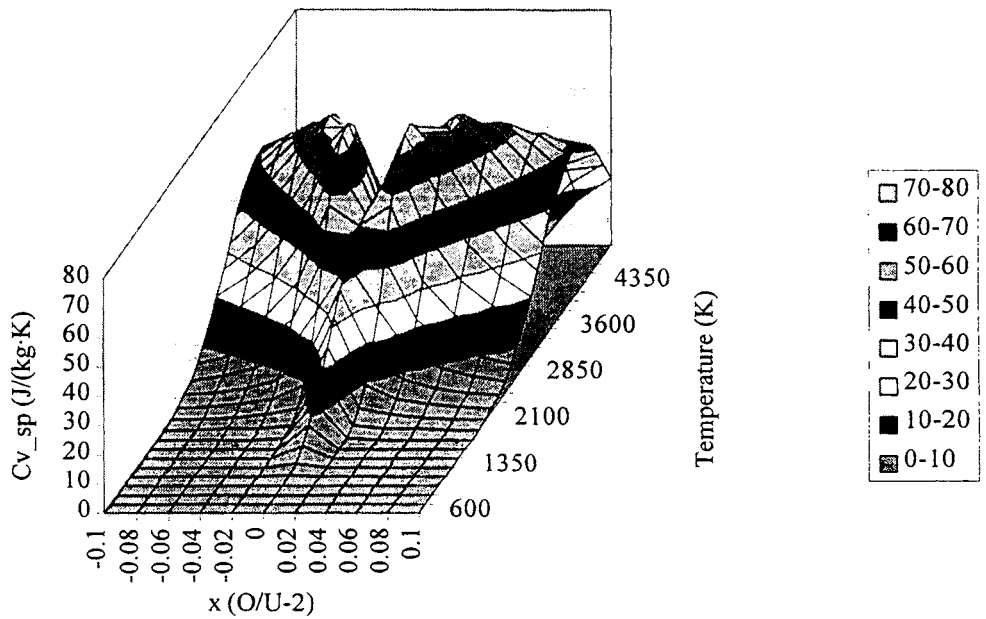


Figure 4: Heat Capacity due to Small Polarons as a Function of Temperature and Stoichiometric Deviation

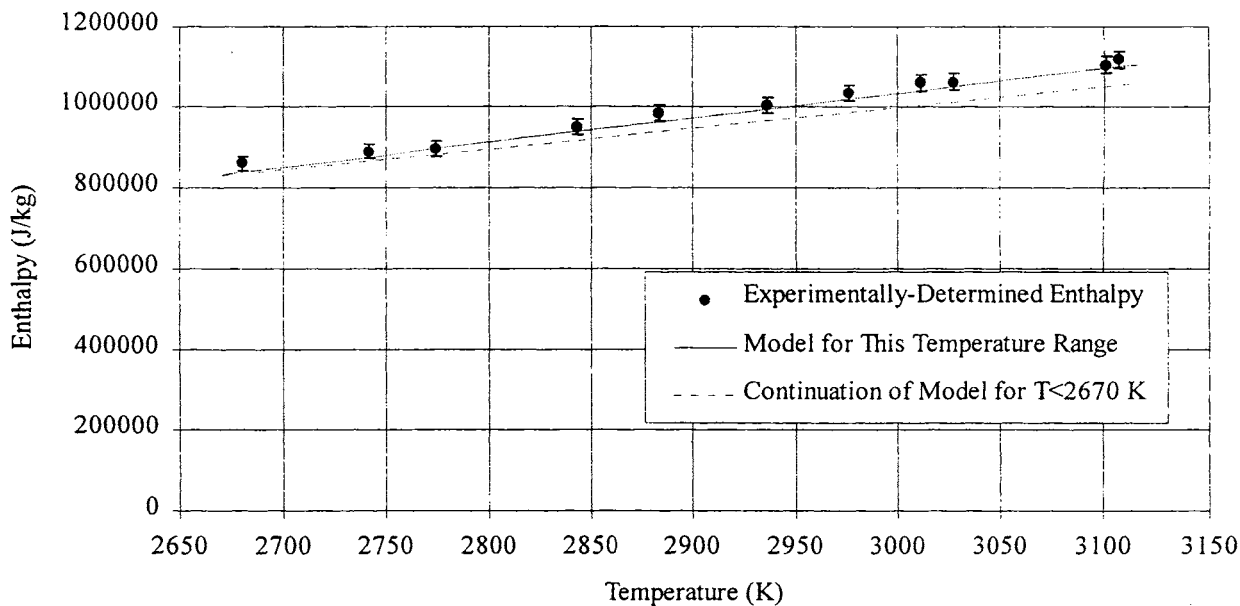


Figure 5: Hein & Flagella's Enthalpy Data for Solid  $UO_{2.003}$  Above 2670 K, Model Used for this Temperature Range and Extrapolation of Model for  $T < 2670$  K

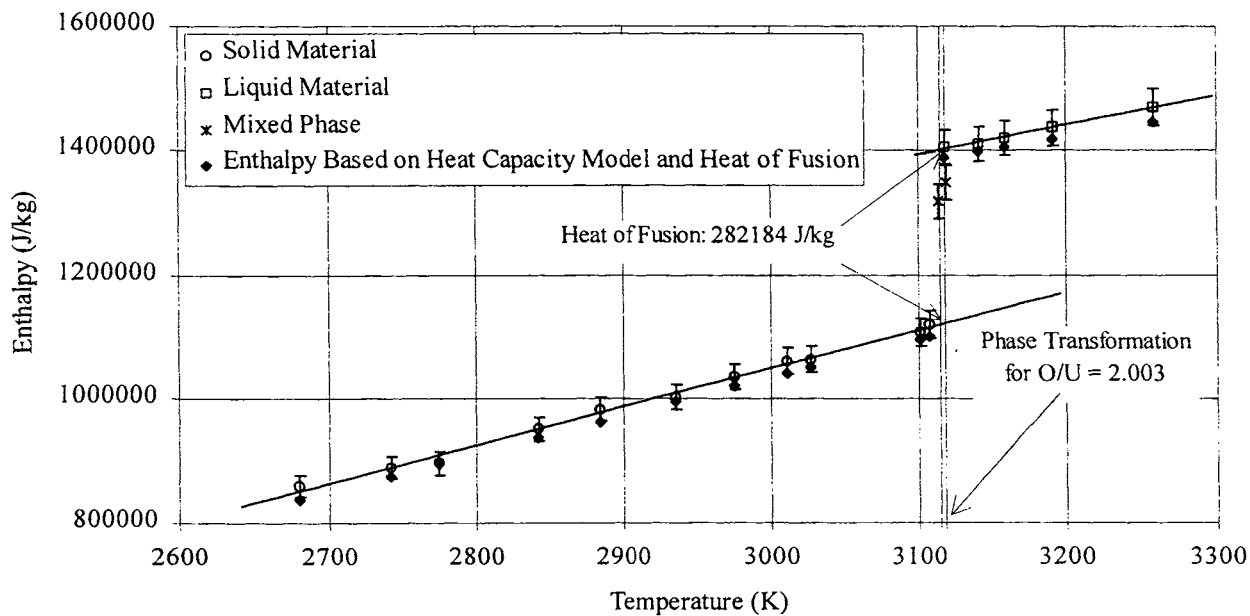


Figure 6: Heat of Fusion for Near-Stoichiometric  $UO_2$  Based on the Enthalpy Data of Hein and Flagella

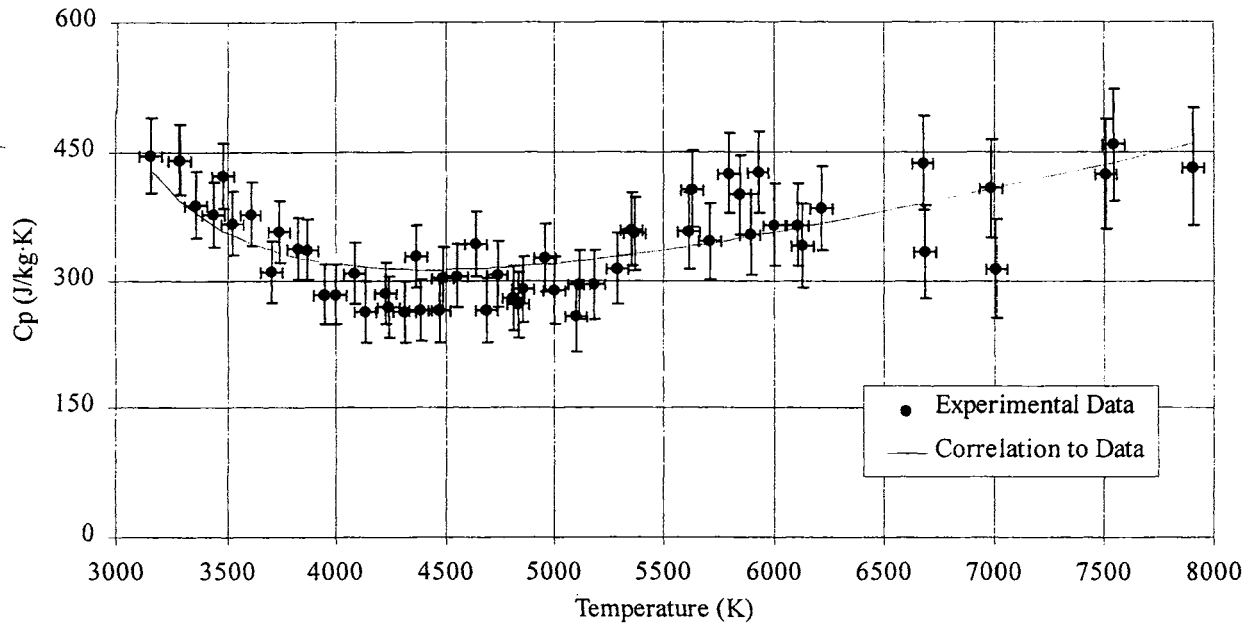


Figure 7: Heat Capacity of Molten  $\text{UO}_2$  (Ronchi *et. al.*) and Model for Molten Fuel

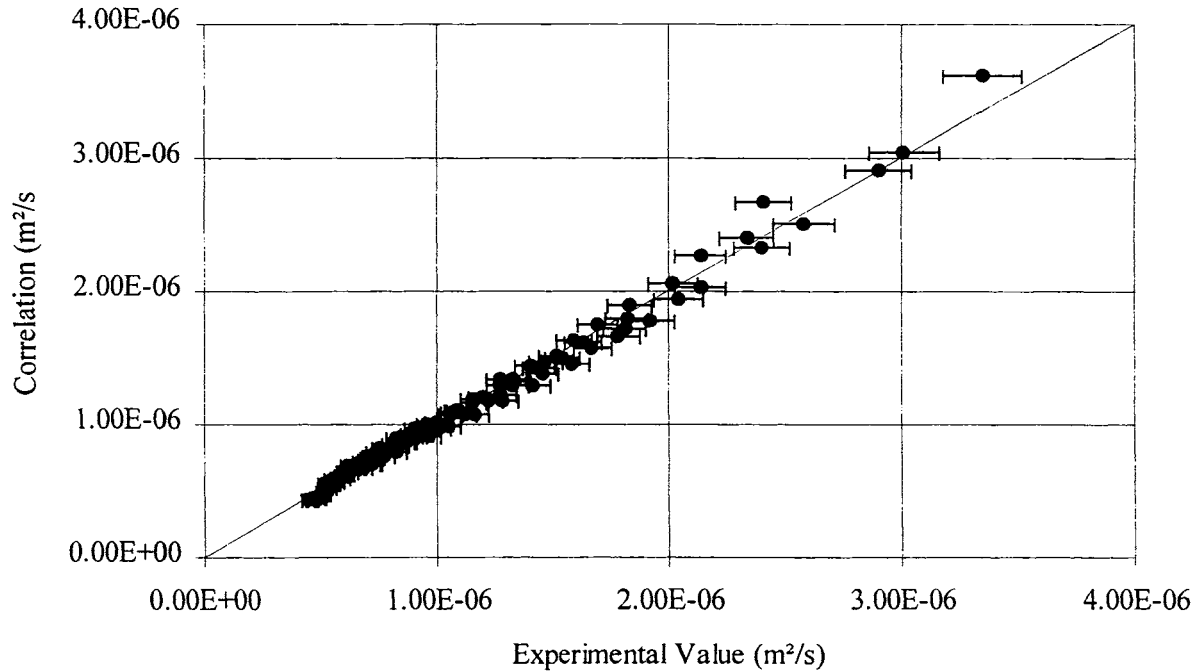


Figure 8: Predicted Thermal Diffusivity from Equation ( 22 ) vs. Data from Reference [20]

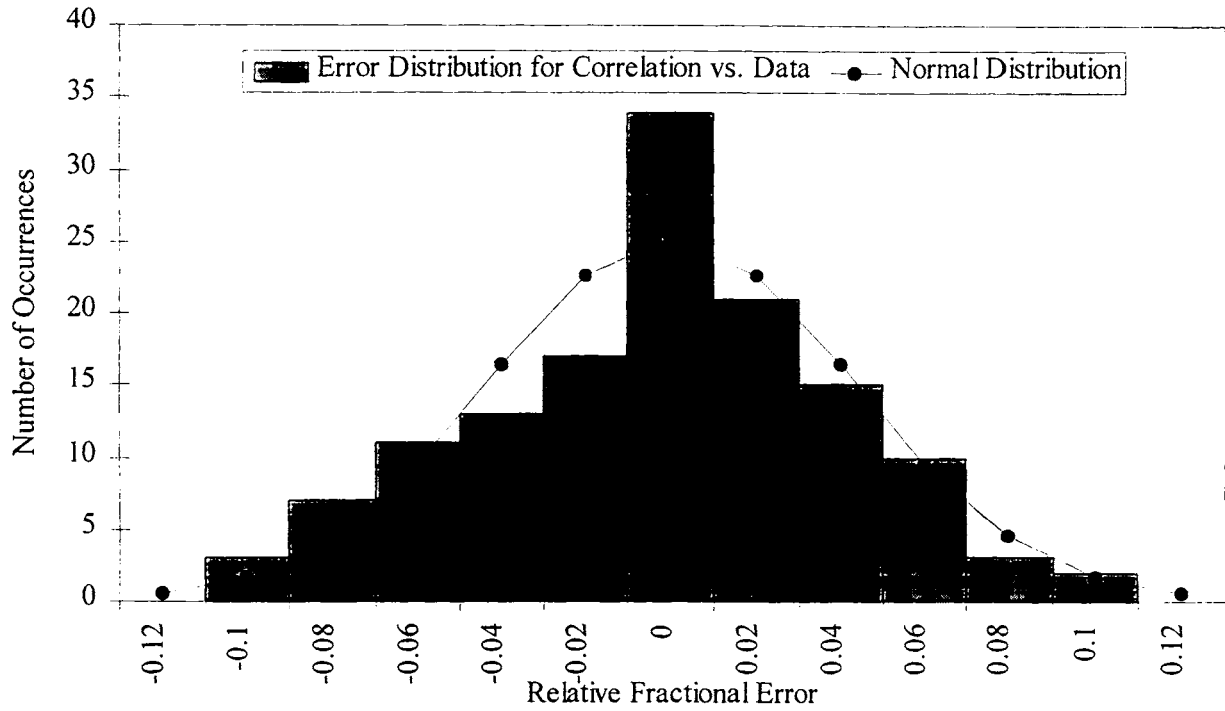


Figure 9: Comparison of Error Distribution from Comparison of Equation ( 22 ) to the Data in Reference [20] With the Normal Distribution (all data used)

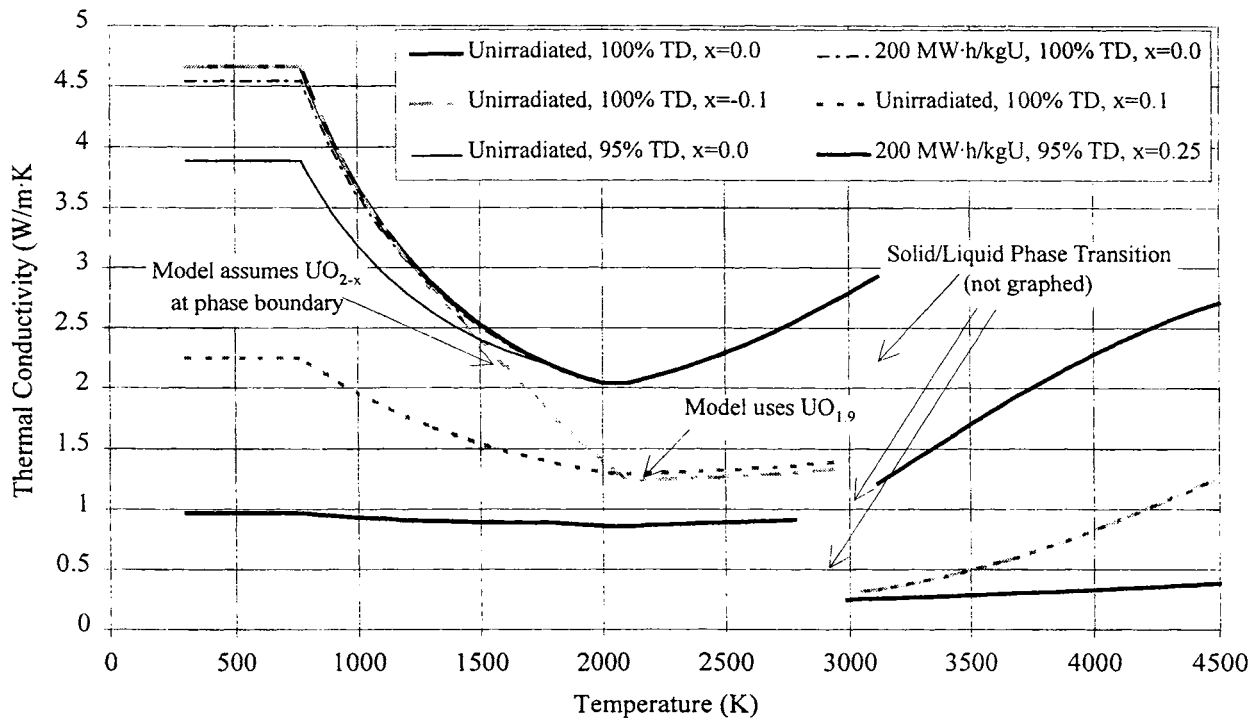


Figure 10: Thermal Conductivity of  $UO_{2-x}$ , According to the Model Presented in this Document